RESEARCH ARTICLE

Characteristics of Nepartak (2021), a subtropical cyclone controlled by an upper-tropospheric cutoff low

Kenta Irie[1] ⓘ | Tetsuya Takemi[2] ⓘ

[1]Graduate School of Science, Kyoto University, Kyoto, Japan

[2]Disaster Prevention Research Institute, Kyoto University, Kyoto, Japan

Correspondence
Kenta Irie, Disaster Prevention Research Institute, Kyoto University, Gokasho, Uji, Kyoto 611-0011, Japan.
Email: irie_k@storm.dpri.kyoto-u.ac.jp

Abstract

This study investigated the structural and track change of cyclone Nepartak occurred over the western North Pacific in July 2021, a cyclone appeared at the surface level, using ERA5 data, focusing on the relationship with an upper-tropospheric cutoff low (COL). The COL was shown to dominate the structural change of Nepartak which developed as a subtropical cyclone with a hybrid structure. As the surface cyclone approached the COL, it was overlapped by the COL and became a cyclone with a two-storied structure, resulting in its abrupt track change. An analysis of the potential vorticity (PV) tendency showed that the movement of Nepartak toward the COL ceased because of the counter-balance of the horizontal/vertical PV advection with the PV anomaly generated by diabatic heating, whereas the surface cyclone northward motion was primarily due to the horizontal PV advection associated with the COL. Nepartak is a case in which changes in the structure and track of a cyclone are controlled by a COL.

KEYWORDS
cutoff low, extratropical weather systems, hybrid cyclone, subtropical cyclone

1 | INTRODUCTION

Nepartak, which was analyzed as a tropical storm by Japan Meteorological Agency (JMA) in the western North Pacific (WNP) in 2021, formed at 1200 UTC July 23, 2021 and made landfall in Miyagi Prefecture (yellow area in Figure 1a) from the Pacific Ocean side at 2100 UTC July 27, 2021. After landfall, the cyclone moved westward and reached the Sea of Japan, transforming into an extratropical cyclone at 0600 UTC July 28. The minimum central pressure and maximum wind speed during its lifetime were 990 hPa and 20 m s^{-1}, respectively (Figure 1b). Although Nepartak was not an intense storm, its approach toward the Japanese main island had

social impacts, such as forcing some events of the Tokyo Olympic games to be rescheduled.

Only one tropical cyclone (TC) had previously made landfall in the Tohoku region in Japan from the North Pacific Ocean side: Typhoon Lionrock (2016). Thus, Nepartak is the second TC that took this track in the observational history of JMA. The counterclockwise track of Lionrock (2016) before landfall was shown to be affected by the influence of an upper-tropospheric cutoff low (COL) (Yoshino et al., 2017). A COL is a low-pressure system with a cold core in the upper troposphere that is cutoff from the jet stream or the mid-Pacific trough (Kasuga et al., 2021; Nieto et al., 2005, 2008). A COL was also shown to impact the TC track of Typhoon Jongdari
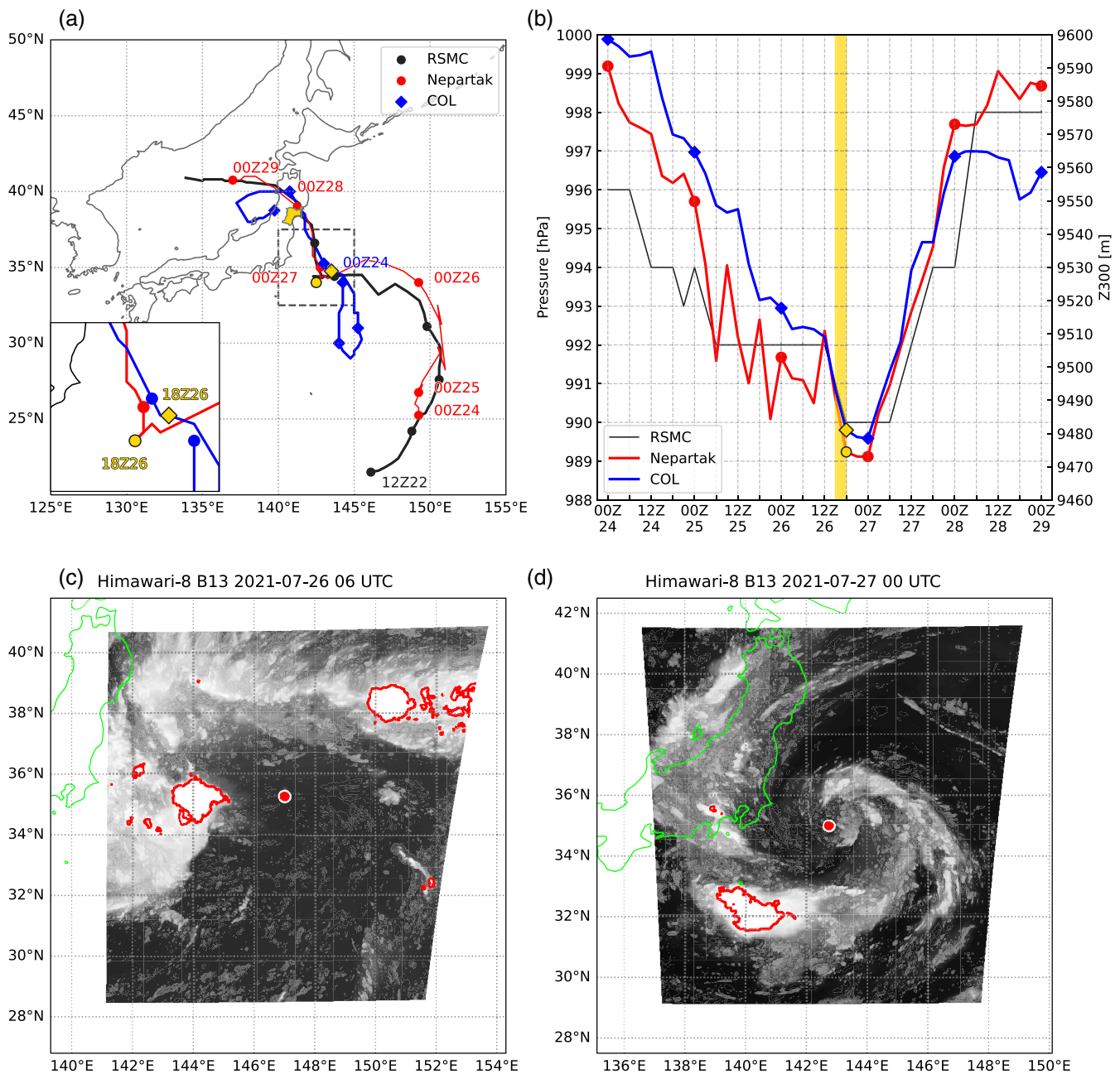
FIGURE 1 (a) The observed track (black line) of Nepartak from the JMA best-track data and the tracks of Nepartak (red line) and the COL (blue line) calculated from ERA5 data. (b) The time series of SLP (hPa) of Nepartak in the best track (black line) and ERA5 (red line) and of the Z300 (m) of the COL (the blue line). The red dots (blue diamonds) indicate the Nepartak (COL) centers at 0000 UTC or 1200 UTC of each day. The vertical yellow band indicates the period from 1500 UTC July 26 to 1800 UTC July 26 and the yellow circle (diamond) indicates the period at 1800 UTC July 26. (c), (d) Infrared image (band 13) from the Himawari-8 satellite (shaded, K) at 0600 UTC July 26 and 0000 UTC July 27. The red contour indicates the brightness temperature at 220K. The red dots with a white edge indicate the Nepartak center. COL, cutoff low; JMA, Japan Meteorological Agency; SLP, sea-level pressure.

(2018) (Wada et al., 2022; Yan et al., 2021). The steering flow and the position of the North Pacific High were shown to have affected the track of these typhoons. For the case of Nepartak, a COL was located to the north of it at its early stage; during the cyclonic movement of it, a COL was located to the west of the storm. Because some studies showed that COLs affected the seemingly unusual tracks of cyclones, the COL is considered to have played a role in determining the track of Nepartak.

An interesting point for Nepartak is that its cloud pattern, as observed from Himawari-8 (Figure 1d), appears to be atypical of a TC but similar to the cloud pattern of a

subtropical cyclone (Evans & Guishard, 2009; Guishard et al., 2007, 2009; Yanase & Niino, 2018). Previously subtropical cyclones that occurred in the Atlantic Ocean, in the Hawaii region, and in the Mediterranean Sea were investigated in relation to COLs (da Rocha et al., 2019). Despite potentially frequent encounters of TCs with COLs in the WNP, only a few studies have investigated the relationship between a subtropical cyclone and a COL in controlling the cyclone track over this region. Ogura et al. (2005, 2009) examined subtropical cyclone cases over Japan; however, their focus was to investigate subtropical cyclones themselves.

Another interesting point of Nepartak is that its track abruptly changed northward from westward at 1800 UTC July 26 (yellow dot in Figure 1a). Some studies examined an abrupt northward change of a TC track in relation to a monsoon gyre (Ge et al., 2018; Ito et al., 2020; Liang & Wu, 2015). Liang and Wu (2015) investigated TCs with and without a northward track change to the east of monsoon gyres and found that the merging of TCs with monsoon gyres is a key to cause sudden track changes of TCs. Their studies, however, did not examine the impact of an upper-level trough on the cyclone motion.

This study focuses on the aforementioned COL for its role in the abrupt change of the Nepartak track. The purpose of this study is to document the characteristics of the structure and the track of the cyclone and to examine how the COL impacted the cyclone track.

2 | DATA AND ANALYSIS METHODS

2.1 | Data sets and cyclone tracking

The data used are the ERA5 reanalysis (Hersbach et al., 2020) having a horizontal resolution of $0.25° \times 0.25°$ with 37 vertical layers and a time interval of 3 h. This high spatiotemporal resolution is useful in capturing the cyclone structure. The analysis period is from 1800 UTC July 23, 2021 to 2100 UTC July 28, 2021. The locations of Nepartak and the COL centers are determined with the use of sea-level pressure (SLP) and the geopotential height at the 300 hPa level (Z300), respectively. The centers of Nepartak and the COL at time T (hour) were identified at points having the local minima of SLP and Z300, respectively, in a $2° \times 2°$ box. The local minima at time $T+3$ (h) are found over an area within a radius of 500 km from the center at time T (h). The central location at time $T+3$ are determined at a point having the smallest distance from the center at time T.

The initial central location of Nepartak is set to the position determined in the best-track data of JMA, which are also used to validate the track of the cyclone determined by this analysis. Precisely, the initial central location is determined as a point having the local SLP minimum to the best-track center. The tracks of Nepartak and the COL determined from the ERA5, as well as the best track, are shown in Figure 1a. Although some fluctuating movements are observed in the track identified from the cyclone tracking procedure, our analysis captures well the movement of the cyclone. Figure 1b shows the temporal variation of the central pressure of Nepartak. The central pressure identified from the ERA5 reaches its minimum at 2100 UTC July 26, and the pressure starts to increase earlier than that of the best track. The central height of the COL is also shown in Figure 1b. The change in height of the COL center appears to be in phase with that of Nepartak.

2.2 | Cyclone diagnosis

The cyclone phase space (CPS; Evans & Hart, 2003; Hart, 2003) is used to diagnose the structural changes of Nepartak. Although the CPS analysis was originally developed for Atlantic cyclones, it was found to be applicable for WNP cyclones (e.g., Bieli et al., 2019a, 2019b; Kitabatake, 2011; Kitabatake & Bessho, 2008). The cyclone parameters are calculated at each time step with data over a circular area within a 500 km radius from the Nepartak center, following the method of Evans and Hart (2003). Data at the 900, 600, and 300 hPa levels are used to calculate the lower- and upper-level parameters. The cyclone parameters are

$$B = h\left[\overline{(Z_{600} - Z_{900})}\Big|_R - \overline{(Z_{600} - Z_{900})}\Big|_L \right], \quad (1)$$

$$-V_T^L = \frac{\partial \Delta Z}{\partial p}\Big|_{900}^{600} = \frac{(Z_{max} - Z_{min})_{600} - (Z_{max} - Z_{min})_{900}}{\ln P_{600} - \ln P_{900}}, \quad (2)$$

$$-V_T^U = \frac{\partial \Delta Z}{\partial p}\Big|_{600}^{300} = \frac{(Z_{max} - Z_{min})_{300} - (Z_{max} - Z_{min})_{600}}{\ln P_{300} - \ln P_{600}}, \quad (3)$$

where B is the thermal symmetry in the lower layer, $-V_T^L$ is the lower-layer thermal structure, and $-V_T^U$ is the upper-layer thermal structure. Here, $h = 1$ in the Northern Hemisphere, Z is the isobaric surface height, and subscripts R and L indicate the right and left sides of the direction of cyclone movement, respectively.
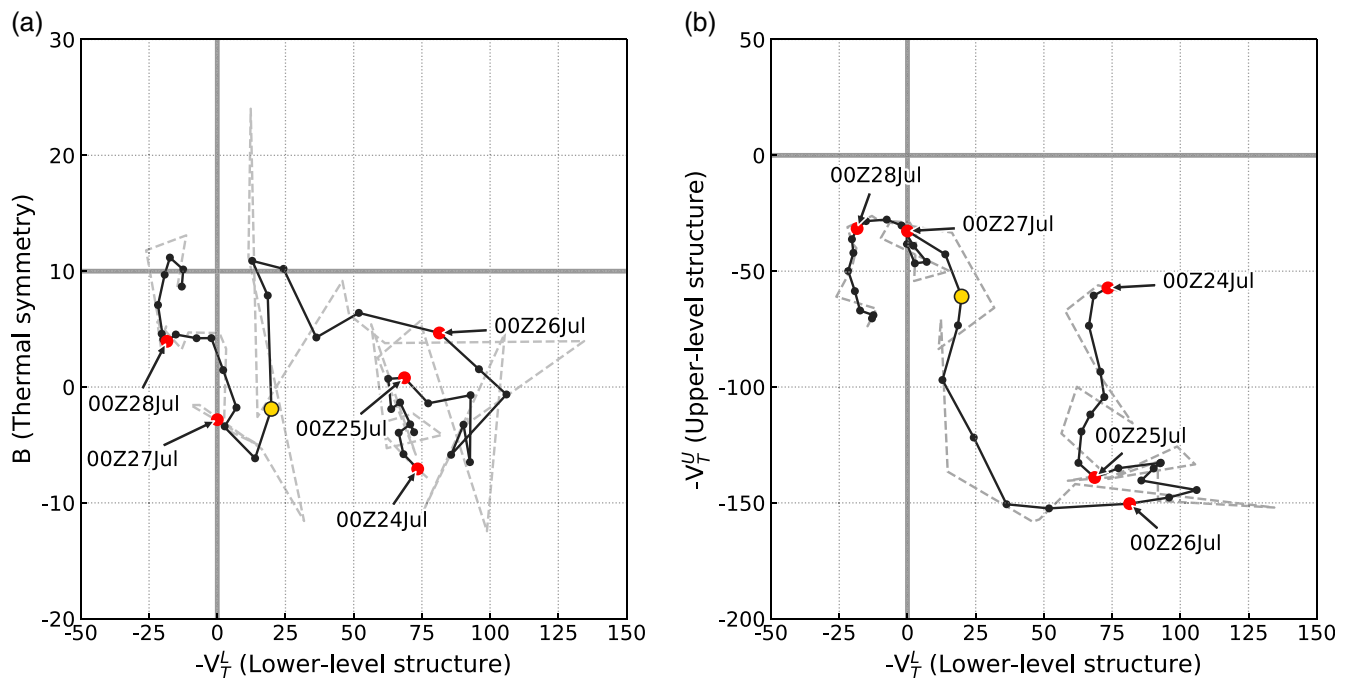
FIGURE 2 The structural change of Nepartak from 0000 UTC July 24 to 2100 UTC July 28 in cyclone phase space with (a) B versus $-V_T^L$ and (b) $-V_T^L$ versus $-V_T^U$. The black solid line shows the 6 h moving average value of the cyclone parameter, and the gray broken line shows the raw value. The red dots denote the time at 0000 UTC and 1200 UTC on each day, and the yellow dot denotes the time at 1800 UTC July 26.

Subscript numbers (i.e., 300, 600, and 900) refer to pressure levels. A cyclone is characterized as a symmetric structure when $-10 < B < 10$ and a hybrid structure when $-V_T^L > -10$ and $-V_T^U < 10$ (Evans & Guishard, 2009).

3 | SUBTROPICAL CYCLONE CHARACTERISTICS

First, the structural features of Nepartak are examined. The thermal structure in the lower layer is shown in Figure 2a. The thermal symmetry B varied between $+10$ and -10 throughout its lifetime (from 0000 UTC July 24 to 2100 UTC July 28). The $-V_T^L$ value is close to 0 at 0000 UTC July 27, indicating a weakening of the lower-layer warm core structure. At this time, the lower-level structure is symmetric ($B \cong 0$), and the cyclone does not undergo a typical structural change from a tropical cyclone to an extratropical cyclone (from $B = 0$, $-V_T^L > 0$ to $B > 10$, $-V_T^L < 0$). Parameters for the upper-level thermal structure are negative throughout the lifetime of Nepartak (Figure 2b), indicating that the cyclone is not a typical TC with a deep warm core. Until approximately 0000 UTC July 27, it exhibits a hybrid structure with a lower warm core structure and an upper cold core structure, consistent with the characteristics of a subtropical cyclone (Evans & Guishard, 2009; Yanase & Niino, 2018).

Therefore, the CPS analysis indicates that Nepartak sustained as a subtropical cyclone from the time of its formation to 1200 UTC July 27.

Figure 3a–d shows the horizontal distributions of equivalent potential temperature (EPT) and geopotential height at the 850 hPa level. At 1800 UTC July 25, Nepartak appears to move northward along the periphery of the high potential vorticity (PV) region (corresponding to the COL) (Figure 3e) and the position of the minimum 850 geopotential height is shifted to the north of the surface cyclone center (Figure 3a). This vertically tilted structure suggests that Nepartak did not have a robust TC structure with upright eyewall clouds (not shown). High-EPT air masses are distributed near the cyclone center (Figure 3a), corresponding to a lower-level warm core structure. At 0600 UTC July 26 (Figure 3b), Nepartak moves northwestward, with higher-EPT air masses to the north and east of its center. Lower-EPT air is advected from northwest to southwest of its center, indicating a frontal structure (Figure 3b). The region of high horizontal EPT gradient to the west of the cyclone center corresponds to a region of active convection according to the Himawari-8 imagery (Figure 1c). At 1800 UTC July 26 (Figure 3c), the westward movement of the cyclone ceases. Lower-EPT air located southwest of the Nepartak center moves northeastward, surrounding the cyclone center. By 0600 UTC July 27 (Figure 3d), Nepartak starts
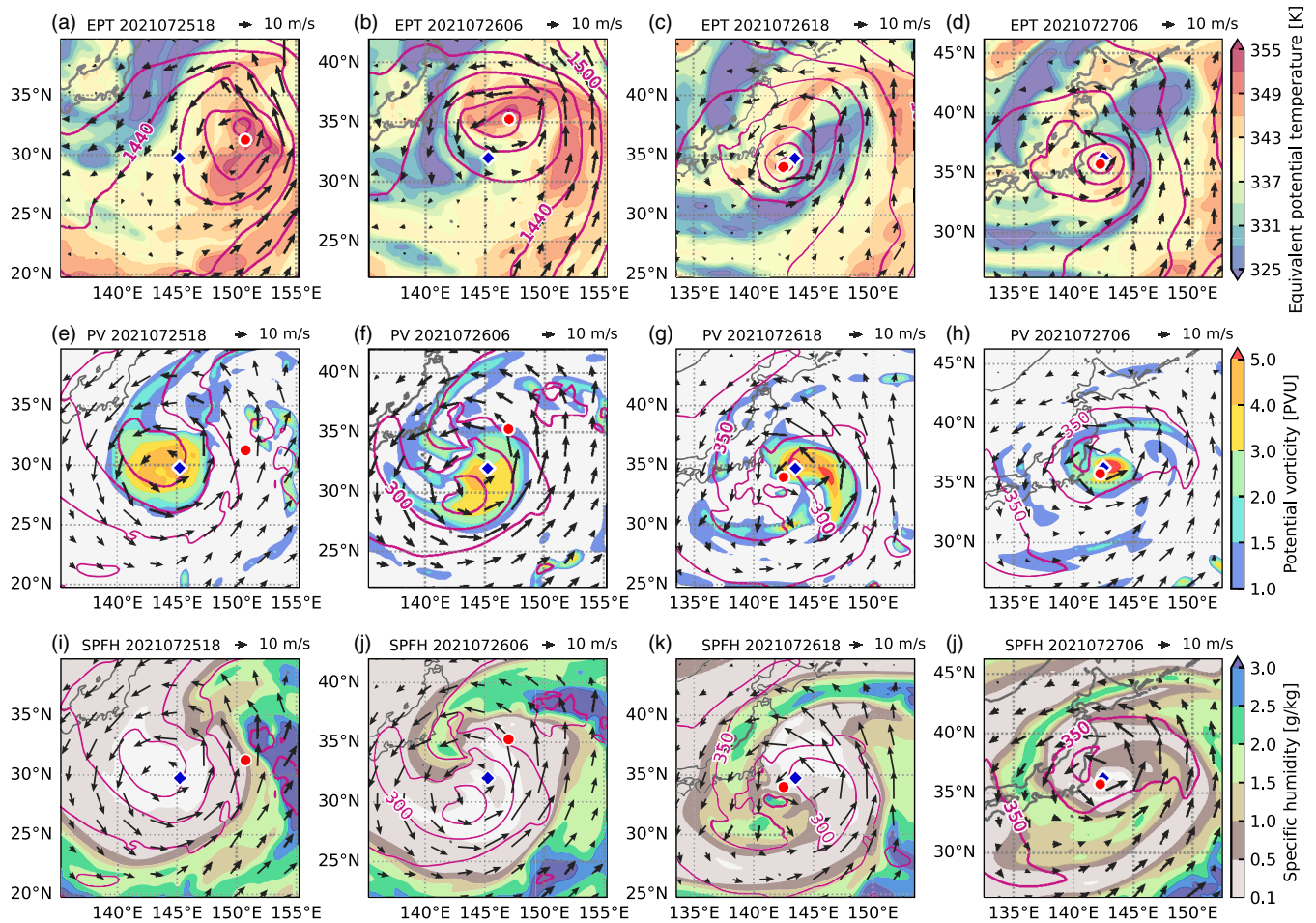
FIGURE 3 (a–d) The horizontal distribution of the EPT (at 2K intervals, shaded), geopotential height (at 30 m intervals, contoured), and wind (m s^{-1}, vector) at the 850 hPa level; (e–h) the PV (shaded), pressure (at 50 hPa intervals, contoured), and wind (m s^{-1}, vector) at the 340K isentropic surface; and (i–l) the specific humidity (shaded) and pressure (at 50 hPa intervals, contoured) (bottom row) at (a, e, i) 1800 UTC July 25, (b, f, j) 0600 UTC July 26, (c, g, k) 1800 UTC July 26, and (d, h, l) 0600 UTC July 27. The red dots and blue diamonds indicate the centers of Nepartak and the COL, respectively. EPT, equivalent potential temperature.

to move northward. Lower-EPT air is spiraling into the cyclone center and the higher-EPT air around it is surrounded by the lower-EPT air. The EPT distribution and CPS indicate that the structural change of Nepartak occurred within a 24-h period (from 0000 UTC July 26 to 0000 UTC July 27).

The upper tropospheric motion is diagnosed by isentropic surface analysis; the PV and specific humidity can be regarded as conserved quantities, while flows across the geopotential height contour on an isotrope indicate vertical motions. We focused on the 340K isentrope because this level corresponds to the upper troposphere (200–400 hPa) in this case. The PV (specific humidity) on the 340K isentrope is shown in Figure 3e–h (Figure 3i–l). At 1800 UTC July 25 (Figure 3e), higher-PV air is not seen over Nepartak. In addition, dry air associated with the COL is widespread over the cyclone (Figure 3i). During the period from 0600 UTC July 26 to 0600 UTC

July 27, when it approaches the COL center in a counterclockwise direction, dry air with a higher PV associated with the COL near 250 hPa is observed to descend to 300 hPa at 1800 UTC July 26 (Figure 3f,g,j,k). At 0600 UTC July 27, the dry air with high PV covers Nepartak (Figure 3h,l), which strongly suppressed cloud organization during the period and played a role in preventing its evolution into a TC.

Finally, we examine the tropospheric vertical structure through vertical cross-sections of PV and potential temperature anomalies across the center of Nepartak during the same period as shown in Figure 3 (Figure 4). Here, an anomaly is defined as the difference between a pointwise value and the regional mean (120°–160°E, 20°–55°N). The vertical structure of the cyclone at 1800 UTC July 25 shows a wet (RH ≥ 70%) PV tower (≥ 1 PVU) extending from the surface to around 300 hPa, located to the east of the center (Figure 4a). This wet
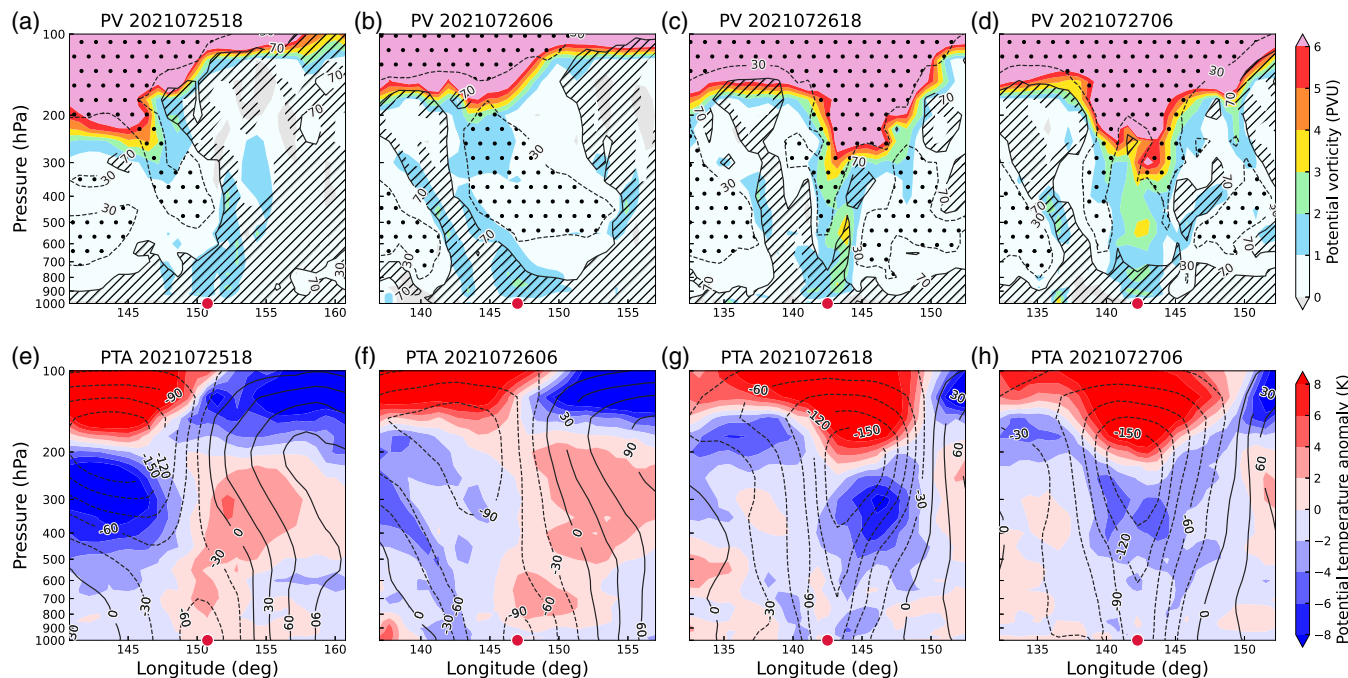
FIGURE 4 (a–d) The vertical cross-section of the PV (shaded, in PVU) and relative humidity (at 30% and 70%, contoured); (e–h) the potential temperature anomaly (shaded, in K) and the geopotential height anomaly (at 30 m intervals, contoured) across the center of Nepartak at (a, e) 1800 UTC July 25, (b, f) 0600 UTC July 26, (c, g) 1800 UTC July 26, and (d, h) 0600 UTC July 27. The dotted (slashed) hatch indicates the dry (wet) region. Red dots denote the central positions of Nepartak. The longitude axes are not standardized, as the figure is drawn within 10° east and west of the center of Nepartak. PV, potential vorticity.

condition is consistent with the area of high convective activity in the eastern side of the cyclone (not shown). A wet (dry) low-level atmospheric column with low PV is identified over the center of Nepartak (Figure 4a). In addition, a warm region is observed from 700 to 300 hPa (Figure 4e). Negative potential temperature and geopotential height anomalies on the west side of 145°E correspond to cold air associated with the COL. At 0600 UTC July 26, the cyclone core region has PV (values over 1 PVU) (Figure 4b) and an expanding warm anomaly (Figure 4f). A narrow PV tower located to the west of the cyclone center (143°E) is associated with active convection (Figure 1c) and is a moist layer from low to mid levels (Figure 4b), whereas the central PV core is only moist at low levels. In addition, the central PV core (≥ 1 PVU) associated with Nepartak appears to be overlapped by a higher-PV region associated with the COL (Figure 4b). Furthermore, cold air associated with the COL continues to be observed around 140°E (Figure 4f). At 1800 UTC July 26, a PV tower extending from the lower to the upper troposphere appears at Nepartak's center (Figure 4c), and the cyclone's warm core weakens (Figure 4g). This is a situation where the low-level PV is completely overlapped by the upper-level PV and is regarded as a two-storied, single cyclone. This two-storied low-pressure system exhibits a barotropic structure,

which becomes more significant at 0600 UTC July 27 (Figure 4d,h). This structural change from 0000 UTC July 26 to 0000 UTC July 27 also appears in the CPS, where the thermal structure of the cyclone transits from the lower-right to the lower-left quadrant (Figure 2b).

In summary, Nepartak has initiated as a symmetric hybrid structure moved into a COL and was overlapped by a COL. Finally, the cyclone moved northward as a unique synoptic low-pressure system having a two-storied structure.

4 | POLEWARD TRACK CHANGE

Nepartak changed its course at 1800 UTC July 26 (yellow dot in Figure 1a) since before that, it moved westward due to the influence of the COL circulation. The values of D denoted in Figure 5a,d indicate the horizontal distance between the centers of the cyclone and the COL. Nepartak gradually approaches the COL: from 124.1 km at 1800 UTC July 26 (Figure 5a) to 60 km at 0600 UTC July 27 (Figure 5d). As described in Section 3, the overlapping of Nepartak and the COL as a barotropic system is considered to affect the moving direction of the surface cyclone. To diagnose the change of the cyclone track before and after 1800 UTC July 26, we examine the PV
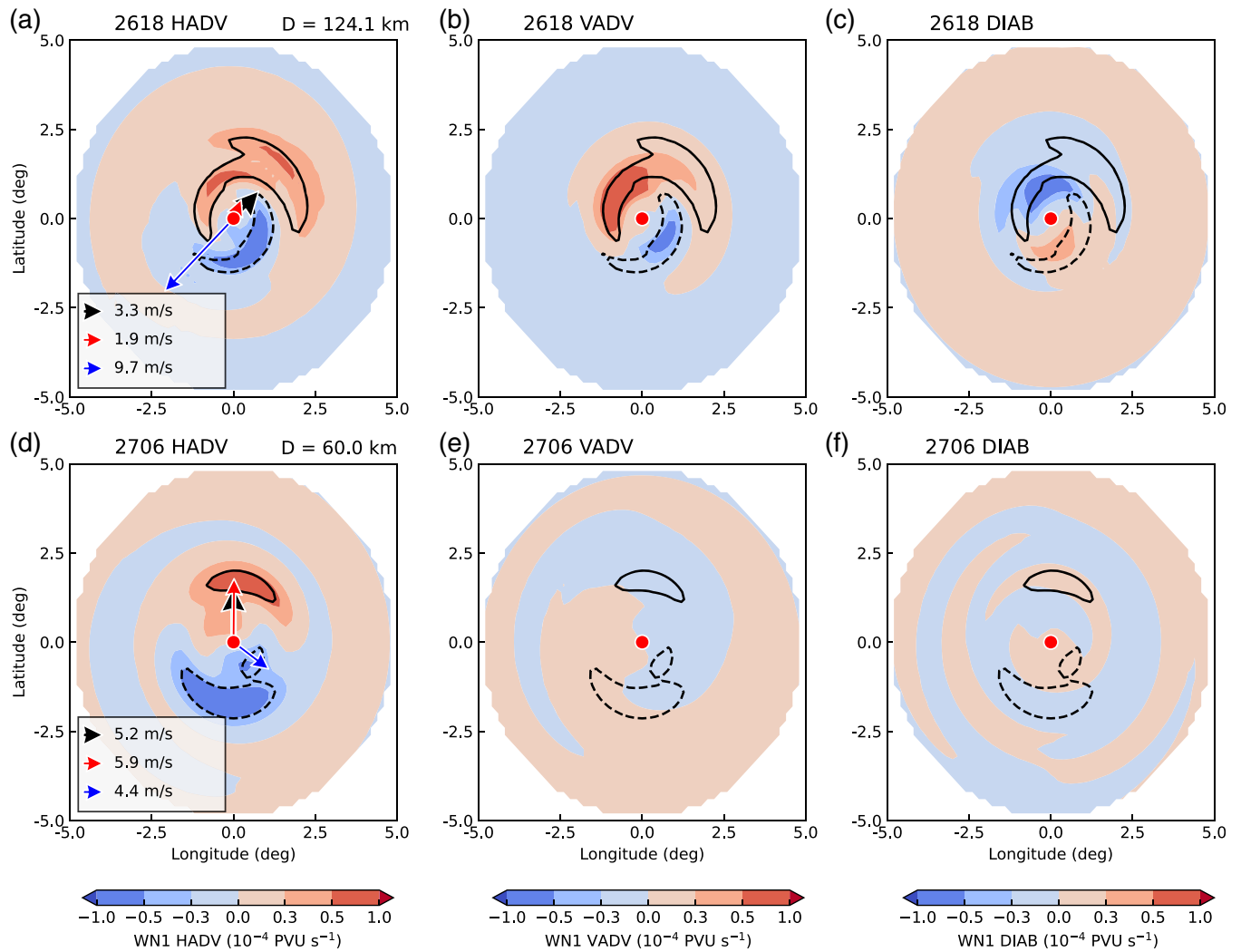
FIGURE 5 The horizontal distributions of the WN-1 component of the 300–700 hPa layer mean PV tendency (at ± 0.5 PVU, contoured) for HADV (at $\pm 5 \times 10^{-4}$ PVU s^{-1}, shaded) (left panel), VADV (at $\pm 5 \times 10^{-4}$ PVU s^{-1}, shaded) (middle panel), and DIAB (at $\pm 5 \times 10^{-4}$ PVU s^{-1}, shaded) (right panel) at (a–c) 1800 UTC July 26 and (d–f) 0600 UTC July 27. The value of D at each time is denoted at the top of the left panels. The black, red, and blue vectors indicate the movement vector, the steering flow vector, and the vertical wind shear, respectively. The specific values of each vector are denoted inside figures (a) and (d), which reflect the length of vectors. Red dots denote the central positions of Nepartak. HADV, horizontal advection; PV, potential vorticity; VADV, vertical advection.

tendency by focusing on the wavenumber-1 (WN-1) (Chan et al., 2002; Wu & Wang, 2000). Examining the WN-1 component of the PV tendency, a cyclone is diagnosed to move toward the region of positive PV. Using the PV equation in the p-coordinate system (Chan et al., 2002; Wu & Wang, 2000), the equation for cyclone movement can be written as:

$$-\boldsymbol{C} \cdot \boldsymbol{\nabla} q_s = \frac{\partial q_1}{\partial t} = \Lambda_1 \left\{ -\boldsymbol{V} \cdot \boldsymbol{\nabla} q - \omega \frac{\partial q}{\partial p} \right.$$
$$\left. -g\left(\zeta_a \frac{\partial H}{\partial p} + \frac{\partial u}{\partial p}\frac{\partial H}{\partial x} - \frac{\partial v}{\partial p}\frac{\partial H}{\partial y}\right) - F \right\},$$

$$(4)$$

where C is the cyclone motion vector, q_s is the symmetric component of PV, q_1 is the WN-1 component of PV, ζ_a is the absolute vorticity, H is the diabatic heating rate, F is the friction, Λ_1 is the operator to extract the WN-1 component, and $\nabla = \partial/\partial x + \partial/\partial y$ is the horizontal gradient operator. The first, second, third, and fourth terms on the right-hand side of Equation (4) indicate the horizontal advection (HADV), the vertical advection (VADV), the adiabatic heating (DIAB), and the friction (FRIC), respectively. Because we are not able to obtain variables for diabatic heating from the ERA5 data, we estimate DIAB according to the equation used by Emanuel et al. (1987) and Tamarin and Kaspi (2016):

$$H = \frac{d\theta}{dt} = \omega \left(\frac{\partial \theta}{\partial p} - \frac{\Gamma_m}{\Gamma_d} \frac{\theta}{\theta_e} \frac{\partial \theta_e}{\partial p} \right), \qquad (5)$$

where ω is the vertical p-velocity, Γ_m is the moist adiabatic lapse rate, and Γ_d is the dry adiabatic lapse rate. Equation (5) expresses the diabatic heating rate due to latent heating, and the condition that ω is negative was used to calculate H.

Figure 5 shows the horizontal distributions of the WN-1 component of the PV tendency averaged in the 300–700 hPa layer for HADV, VADV, and DIAB. Since the analysis is conducted for the free troposphere, the FRIC term is neglected. The steering flow vector (red vector) is generally consistent with the Nepartak movement vector (black vector). The steering flow vector is calculated using 200–950 hPa pressure-weighted mean winds averaged over a 500 km region from the cyclone center (Liang & Wu, 2015).

At 1800 UTC July 26, when Nepartak stops moving, the vertical shear is large (9.7 m s^{-1}, blue vector), indicating an unfavorable environment for tropical transition (Davis & Bosart, 2003). Simultaneously, the steering flow changes northeastward at 1.9 m s^{-1} from westward (Figure 5a). This northeastward shift of the steering flow is due to the effect of the COL which overlaps the surface cyclone. At 0600 UTC July 27 (Figure 5d), the movement direction coincides with the northward steering flow. The movement of Nepartak appears to be explained by the steering flow, as described in the following discussion.

The movement direction of Nepartak is examined in terms of the PV tendency. Figure 5 shows that the spatial patterns of HADV and VADV appear similar and that DIAB pattern shows an opposite tendency to HADV and VADV patterns at 1800 UTC July 26. Both HADV and VADV show a positive and negative PV tendency around the center, with a positive (negative) tendency on the northwest (southeast) side (Figure 5a,b); by contrast, the distributions of the positive and negative patterns in DIAB are opposite. Overall, the motion vector is directed toward the positive areas of HADV and VADV. The summation of HADV and VADV exceeds the opposite influence from DIAB, and a comparison between HADV and VADV indicates that HADV is larger (Figure 5a,b,d,e). At 0600 UTC July 27, positive HADV areas around the center are located on the north side, which affects the movement direction of Nepartak at these times. In this way, HADV related to the PV of the COL contributes substantially to the translation, suggesting that the movement can be explained by the steering flow.

At 1800 UTC July 26, positive VADV is observed on the northwest side (Figure 5b), whereas positive DIAB appears on the southeast side (Figure 5c). A lower-level PV generated by the latent heat in the convective area to the south of the cyclone is reflected in this DIAB. A positive VADV indicates a northwestward forcing, whereas a positive anomaly of DIAB will change the direction southeastward. Because of the contribution from DIAB, the northwestward forcing by HADV and VADV is suppressed. Therefore, the influences from DIAB are considered to contribute to the slowing of Nepartak. After 1800 UTC July 26, the overall PV tendency shows a northward component because of HADV, which corresponds to the steering flow; the poleward translation is therefore driven (Figure 5d).

Some studies indicate that the abrupt northward track changes of cyclones can be explained by the relationship with monsoon gyres. In the Nepartak case, cyclonic circulation in the subtropic region of the WNP seemed not to be significant (not shown), and therefore, the low-level contribution that may result from a monsoon gyre or other a low-pressure system is not considered to play a role in controlling the abrupt change of the cyclone. Therefore, we focus on the impact of the COL.

5 | CONCLUSIONS

Using the ERA5 data set, we investigated the structural and track change of Nepartak in July 2021 and how it was influenced by a COL. The cyclone experienced an abrupt track change from the westward to the northward direction.

The results indicated that the cyclone, before its abrupt track change, had a hybrid structure consisting of an upper-level cold core and a lower-level warm core. This hybrid structure is due to a strong shear and a cold-air mass of a COL, which suppresses the evolution toward a TC, enabling Nepartak to be regarded as a subtropical cyclone.

As Nepartak approaches nearby COL, it is overlapped by the COL and became a two-storied cyclone, which is diagnosed by PV structures. After this structural change, the cyclone has a low-level cold core as well as the upper-level cold core, and suddenly changes its track to northward. In this way, the presence of the COL plays a critical role in controlling the changes in the structure and track of the cyclone.

The abrupt track change was diagnosed by analysis of the 300–700 hPa multi-level mean PV tendency for the WN-1 component. The cease of the westward movement results from the dominant contribution from the southeastward forcing due to DIAB, whereas the abrupt northward movement is due to HADV contribution mainly from the COL.

Nepartak is a subtropical cyclone—a hybrid of a low-level warm core and an upper-level cold core—which has not been well reported around Japan. The structure and track of it are under the control of a COL by becoming a two-storied structure. Future studies may need to investigate the relationship between a COL and a subtropical cyclone from a statistical viewpoint to enable robust characterization of subtropical cyclones in the WNP.

AUTHOR CONTRIBUTIONS

Kenta Irie: Conceptualization; formal analysis; investigation; methodology; validation; visualization; writing – original draft. **Tetsuya Takemi:** Funding acquisition; supervision; validation; writing – review and editing.

ACKNOWLEDGEMENTS

CONFLICT OF INTEREST STATEMENT

The authors declare no conflict of interest.

DATA AVAILABILITY STATEMENT

The ERA5 data used in this study are available from https://cds.climate.copernicus.eu/cdsapp#!/dataset/reanalysis-era5-pressure-levels?tab=form and https://cds.climate.copernicus.eu/cdsapp#!/dataset/reanalysis-era5-single-levels?tab=form.

ORCID

Kenta Irie https://orcid.org/0000-0003-3709-0153
Tetsuya Takemi https://orcid.org/0000-0002-7596-2373

REFERENCES

Bieli, M., Camargo, S.J., Sobel, A.H., Evans, J.L. & Hall, T. (2019a) A global climatology of extratropical transition. Part I: characteristics across basins. *Journal of Climate*, 32, 3557–3582.

Bieli, M., Camargo, S.J., Sobel, A.H., Evans, J.L. & Hall, T. (2019b) A global climatology of extratropical transition. Part II: statistical performance of the cyclone phase space. *Journal of Climate*, 32, 3583–3597.

Chan, J.C.L., Ko, F.M.F. & Lei, Y.M. (2002) Relationship between potential vorticity tendency and tropical cyclone motion. *Journal of the Atmospheric Sciences*, 59, 1317–1336.

da Rocha, R.P., Reboita, M.S., Gozzo, L.F., Dutra, L.M.M. & de Jesus, E.M. (2019) Subtropical cyclones over the oceanic basins: a review. *Annals of the New York Academy of Sciences*, 1436, 138–156.

Davis, C. & Bosart, L.F. (2003) Baroclinically induced tropical cyclogenesis. *Monthly Weather Review*, 131, 2730–2747.

Emanuel, K., Fantini, M. & Thorpe, A. (1987) Baroclinic instability in an environment of small stability to slantwise moist convection. Part I: two-dimensional models. *Journal of the Atmospheric Sciences*, 44, 1559–1573.

Evans, J.L. & Guishard, M.P. (2009) Atlantic subtropical storms. Part I: diagnostic criteria and composite analysis. *Monthly Weather Review*, 137, 2065–2080.

Evans, J.L. & Hart, R.E. (2003) Objective indicators of the life cycle evolution of extratropical transition for Atlantic tropical cyclones. *Monthly Weather Review*, 131, 909–925.

Ge, X., Yan, Z., Peng, M., Bi, M. & Li, T. (2018) Sensitivity of tropical cyclone track to the vertical structure of a nearby monsoon gyre. *Journal of the Atmospheric Sciences*, 72, 3958–3974.

Guishard, M.P., Evans, J.L. & Hart, R.E. (2009) Atlantic subtropical storms. Part II: climatology. *Journal of Climate*, 22, 3574–3594.

Guishard, M.P., Nelson, E.A., Evans, J.L., Hart, R.E. & O'Connell, D. G. (2007) Bermuda subtropical storms. *Meteorology and Atmospheric Physics*, 97, 239–253.

Hart, R.E. (2003) A cyclone phase space derived from thermal wind and thermal asymmetry. *Monthly Weather Review*, 131, 585–616.

Hersbach, H., Bell, B., Berrisford, P., Hirahara, S., Horányi, A., Muñoz-Sabater, J. et al. (2020) The ERA5 global reanalysis. *Quarterly Journal of the Royal Meteorological Society*, 146, 1999–2049.

Ito, K., Wu, C.-C., Chan, K.T.F., Toumi, R. & Davis, C. (2020) Recent progress in the fundamental understanding of tropical cyclone motion. *Journal of the Meteorological Society of Japan*, 98, 5–17.

Kasuga, S., Honda, M., Ukita, J., Yamane, S., Kawase, H. & Yamazaki, A. (2021) Seamless detection of cutoff lows and preexisting troughs. *Monthly Weather Review*, 149, 3119–3134.

Kitabatake, N. (2011) Climatology of extratropical transition of tropical cyclones in the Western North Pacific defined by using cyclone phase space. *Journal of the Meteorological Society of Japan*, 89, 309–325.

Kitabatake, N. & Bessho, K. (2008) Cyclone phase of tropical cyclones landfalling in Japan during 2004–2006. *SOLA*, 4, 21–24.

Liang, J. & Wu, L. (2015) Sudden track changes of tropical cyclones in monsoon gyres: full-physics, idealized numerical experiments. *Journal of the Atmospheric Sciences*, 72, 1307–1322.

Nieto, R., Gimeno, L., de la Torre, L., Ribera, P., Gallego, D., García-Herrera, R. et al. (2005) Climatological features of cutoff low systems in the Northern Hemisphere. *Journal of Climate*, 18, 3085–3103.

Nieto, R., Sprenger, M., Wernli, H., Trigo, R.M. & Gimeno, L. (2008) Identification and climatology of cut-off lows near the tropopause. *Annals of the New York Academy of Sciences*, 1146, 256–290.

Ogura, Y., Kumabe, R. & Nisimura, S. (2009) Initiation and evolution of a subtropical low observed near the Japan islands. *Journal of the Meteorological Society of Japan*, 87, 941–967.

Ogura, Y., Niino, H., Kumabe, R. & Nisimura, S. (2005) Evolution of a subtropical low causing severe weather over the Kanto area on 13 October 2003. *Journal of the Meteorological Society of Japan*, 83, 531–550.

Tamarin, T. & Kaspi, Y. (2016) The poleward motion of extratropical cyclones from a potential vorticity tendency analysis. *Journal of the Atmospheric Sciences*, 73, 1687–1707.

Wada, Y., Yanase, W. & Okamoto, K. (2022) Interactions between a tropical cyclone and upper-tropospheric cold-core lows simulated by and atmosphere-wave-ocean coupled model: a case study of typhoon Jongdari (2018). *Journal of the Meteorological Society of Japan*, 100, 387–414.

Wu, L. & Wang, B. (2000) A potential vorticity tendency diagnostic approach for tropical cyclone motion. *Monthly Weather Review*, 128, 1899–1911.

Yan, Z., Ge, X., Wang, Z., Wu, C.-C. & Peng, M. (2021) Understanding the impacts of upper-tropospheric cold low on TS Jongdari (2018) using potential vorticity inversion. *Monthly Weather Review*, 149, 1499–1515.

Yanase, W. & Niino, H. (2018) Environmental control of tropical, subtropical, and extratropical cyclone development over the North Atlantic Ocean: idealized numerical experiments. *Quarterly Journal of the Royal Meteorological Society*, 144, 539–552.

Yoshino, J., Nakata, Y., Furuta, N. & Kobayashi, T. (2017) A numerical analysis on the path of Nepartak Lionrock (2016) using the piecewise potential vorticity inversion technique. *Journal of Japan Society of Civil Engineers, Ser. B2 (Coastal Engineering)*, 73, 493–498 (in Japanese with English abstract).